Application of acoustic Full Waveform Inversion to the synthetic Valhall velocity model

Vincent Prieux[1], *Stéphane Operto*[1], *R. Brossier*[1] *and Jean Virieux*[2]
[1]*Géoazur, Université Nice Sophia Antipolis - CNRS,* [2]*LGIT - Université Joseph Fourier*

SUMMARY

We assess the reliability of 2D acoustic frequency-domain full-waveform inversion to image a shallow-water synthetic velocity model with a gas cloud. The velocity model represents the subsurface in the Valhall oil&gas field. We assess the sensitivity of FWI to the maximum offset in the acquisition, to the free-surface effects and to the accuracy of the starting models that were built by smoothing the true model, by first-arrival traveltime tomography and by stereotomography.

INTRODUCTION

We present an application of 2D acoustic frequency-domain full waveform inversion (FWI) to the synthetic Valhall velocity model. The acquisition describes an Ocean Bottom Cable (OBC) survey. The velocity model exhibits shallow sea bottom (70 m) above a relatively structurally-simple medium that contains low P-wave velocity gas layers. The shallow water depth leads to complex interactions between the primary wavefield and the free-surface multiples that makes FWI more non linear, especially when long-offset data are used in the inversion (Sirgue, 2006). Moreover, building an accurate starting velocity model for FWI in the low-velocity zone (LVZ) created by the gas cloud is a difficult issue. We first illustrate how the use of long-offset data improves the reconstruction of the deep part and the ends of the targeted area thanks to a broader aperture illumination. The non linearities introduced by the long offsets are mitigated by a suitable data preconditioning performed by hierarchic time damping during each mono-frequency inversion (Brossier et al., 2008). The time damping is implemented in the frequency domain by mean of complex-valued frequencies (Brenders and Pratt, 2007b). Second, we compare the FWI models inferred from three different starting models built by depth-dependent smoothing of the true model, first-arrival traveltime tomography (FATT) , [e.g.],(Dessa et al., 2004) and reflection stereotomography (Billette and Lambaré, 1998). FATT led to a sufficiently-accurate starting model for FWI down to a maximum depth of 1.5 km roughly corresponding to the top of the gas cloud but failed to produce an accurate model within the LVZ created by the gas cloud whatever the maximum offset. The stereotomography model is sufficiently accurate for FWI down to a maximum depth of 2.5 km but clealy lacks accuracy at greater depths due to insufficient long offset coverage in the acquisition (maximum offset was 9 km for stereotomography) (Lambaré and Alerini, 2005). The inverted data were computed with the forward problem modeling engine implemented in the FWI code. Application of both acoustic and elastic FWI to elastic data are presented in a companion abstract (Brossier et al., Two-dimensional seismic imaging of the Valhall model from synthetic OBC data by frequency-domain elastic full-waveform inversion, submitted in this issue).

FREQUENCY-DOMAIN FULL-WAVEFORM INVERSION

FWI seeks to use the full information content of the recorded wavefield to build high-resolution models of the subsurface (Tarantola, 1987). Here, 2D acoustic FWI is implemented in the frequency domain (Pratt et al., 1998). Pressure wavefields are computed using a 2D visco-acoustic isotropic finite-difference frequency-domain method (Hustedt et al., 2004). For FWI, the model will be parameterized by the P-wave velocity only. In the frequency domain, multiscale FWI proceeds hierarchically from the low to the high frequencies to incorporate progressively shorter wavelenghts in the model (Sirgue and Pratt, 2004). A second level of data preconditioning can be introduced by limiting the inversion to a subset of arrivals (e.g., Sears et al. (2008)). Such data preconditioning can be applied in the frequency domain by mean of complex frequencies ($\omega + i/\tau$), which is equivalent to damp seismograms in time by $\exp^{-\frac{1}{\tau}(t-t_0)}$ (Sirgue, 2003; Brenders and Pratt, 2007a). τ and t_0 control the strength and the timing of the damping respectively. In the following, we shall use t_0=0s. Applying time damping from the first-arrival time can be viewed as a heuristic way to select aperture angles in the data. Aperture angle is the second parameter in addition to frequency which controls the spatial resolution of FWI (Sirgue and Pratt, 2004). In our algorithm, varying time damping is implemented within a loop over τ embedded in the outer loop over frequencies (Brossier et al., 2008). The τ parameter is progressively increased such that the inversion successively proceeds from the early arrivals to the later arrivals during the iterations of each frequency inversion. Other weightings and regularizations consist of data weighting with offset, Gaussian smoothing of the gradient of the objective function and gradient scaling by the diagonal terms of the Hessian (Sourbier et al., 2009a,b).

APPLICATION TO THE VALHALL MODEL

Valhall is on the central zone of a triassic grabben, which underwent a compressive regime during the upper Creteceous, leading to the Lindesnes ridge (Figure 1). The ridge is overlain by a chalk layer, which traps the harnessed oil. Oil originally comes from underlying jurassic layers but migrated upward through numerous fractures. Another extension phase happened during the tertiary age, leading to a massive sedimentary deposit, within which are trapped several gas layers.

Impact of long offsets and free surface effects in FWI

We first assessed the impact of the long offsets and the free surface on FWI. Nine frequencies between 2 Hz and 15 Hz were successively inverted using fifty iterations per frequency. For all the tests, neither data weighting with offset nor gradient smoothing were applied. The source wavelet is assumed to be known. Both sources and receivers are deployed all along the model. The sources are at a depth of 6 m while the re-

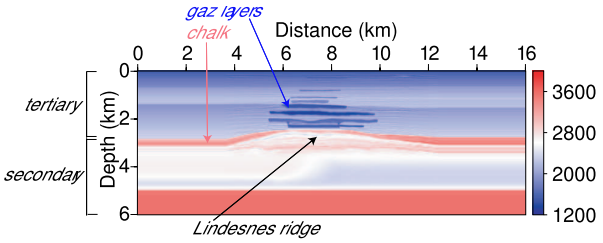

Figure 1: Synthetic Valhall velocity model

ceivers are on the sea bottom. The spacing between sources and between receivers is 50 m. The initial model was built by Gaussian smoothing of the true model with vertical and horizontal correlation lengths of 500 m. An absorbing boundary condition is first implemented on top of the models to compute the inverted and the modeled synthetic data, and no data damping was applied. To assess the effects of long offsets on FWI, we compare FWI models when the maximum offset is 16 km and 32 km (in the later case, the model of Figure 1 was augmented by 8 km on the left and right sides). The final FWI model for the 32-km acquisition closely matches the true one (Figure 2(a)). Comparison between logs of the final FWI models inferred from the 16-km and 32-km acquisitions shows how the long offsets help to reconstruct the deep part and the ends of the target thanks to a broader aperture illumination (Figure 2(b-c)).

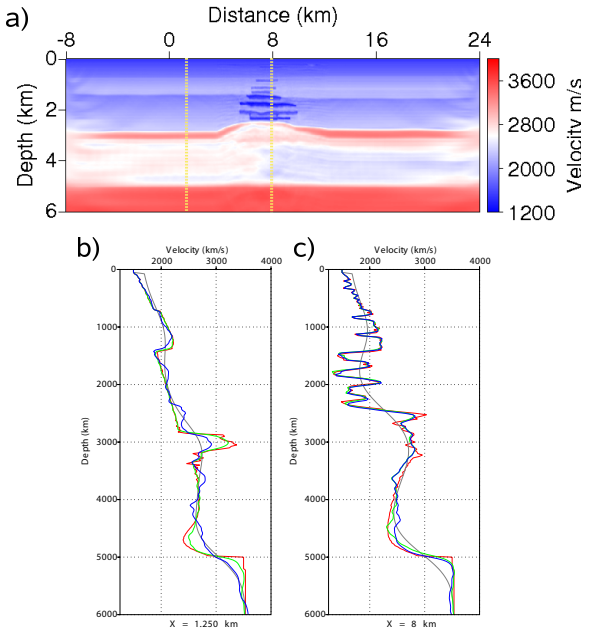

Figure 2: a) Final FWI model for a 32-km acquisition length. The target is between 0 km and 16 km of distance. (b-c) Comparison between logs of FWI models inferred from the 32-km (green lines) and 16-km (blue lines) acquisitions. The logs of the true and of the starting models are plotted in red and gray respectively. b) x=1.25 km. c) x=8 km.

Second, we applied FWI when free-surface boundary condition is implemented on top of the model to compute the inverted and modeled synthetic data. The final FWI model for the 32-km acquisition exhibits some artifacts caused by the non linearities introduced by the free-surface effects when long-offset wave propagations are considered (Figure 3). Then, we applied FWI to damped data using successively τ =0.5, 1, 3 and 6 s during each mono- frequency inversion (Figure 4a). Fifteen iterations were performed for each damping leading to 60 iterations per frequency inversion. The artifacts were mitigated when longer offsets and shorter apertures are progressively introduced in FWI as time damping decreases. Another application of hierarchical time damping for imaging complex onshore structures by joint inversion of body waves and surface waves was presented in Brossier et al. (2008).

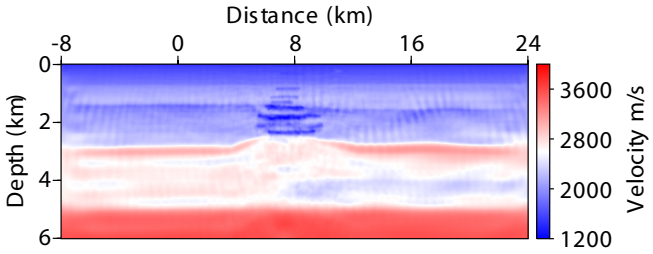

Figure 3: FWI model when a free surface is implemented on top of the model. The maximum offset is 32 km.

To verify that the artifacts were generated by long offsets, we applied FWI for the 16-km acquisition when free surface effects are considered and no data damping is applied. Unlike for the 32-km acquisition, the final FWI model does not exhibit artifacts but remains less accurate in the deep part and near the ends of the target (compare Figures 4a and 4b).

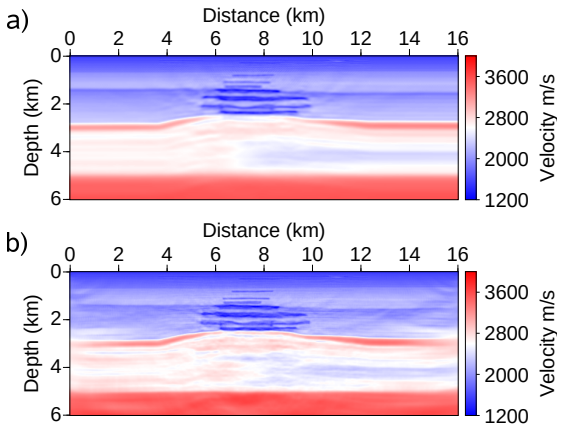

Figure 4: FWI models when a free surface is implemented on top of the model a) Maximum offset is 32 km. Only the 16-km-long targeted zone is shown. Four damping were used τ =0.5, 1, 3 and 6 s. b) Maximum offset is 16 km. No data damping was used.

Influence of the initial velocity models

We assessed the accuracy of different starting models for FWI. Seven frequencies ranging from 4 to 15 Hz were inverted. Free surface is implemented on top of the model. The source wavelet is estimated during the inversion (Pratt, 1999). The acquisition geometry is the same as for the previous tests with a maximum source-receiver offset of 16 km.

The initial velocity models

The first velocity model was built by smoothing the true model with a constant horizontal correlation length of 500 m. The vertical correlation length varied beween 25 m and 1000 m from top to bottom. This smoothing roughly mimics the expected resolution of a velocity model built by FATT. The second initial model was built by FATT for different acquisition lengths (16, 32 and 64 km). Indeed, the maximum offset strongly controls the ray coverage of the subsurface (Figure 5)(a-c). The model to be reconstructed by FATT is a smoothed version of the true model. First-arrival traveltimes to be inverted were computed with an eikonal solver. The initial model for FATT is a velocity gradient model. Velocity logs extracted from the final FATT models are shown in Figures 5(d-e) for the 3 acquisitions. FATT provided an accurate reconstruction down to 1.5 km depth which roughly corresponds to the top of the gas cloud. Below, minor differences are seen between the 3 FATT models, except at depths greater than 6.5 km where the 64-km acquisition provided the correct velocity. FATT failed to accurately position in depth the high-velocity layer at 3-km depth (Figures 5(e)). This failure highlights the limits of FATT when sharp LVZs affect the subsurface. The third starting model for FWI was built by PP-PS stereo-tomography (Lambaré and Alerini, 2005). The stereotomography was applied for an OBC acquisition with a maximum offset of 9 km in the middle of the profile. This maximum offset decreases as the common mid point moves away from the center of the profile. Only the reflected events were picked during stereotomography. The velocity models built with the 3 abovementioned approaches are shown in Figure 6. Comparison of logs extracted from the three velocity models suggests that FATT provides the most accurate model down to the top of the gas cloud while the stereotomography provides the most accurate reconstruction of the gas cloud down to a maximum depth of 3 km (Figure 7).

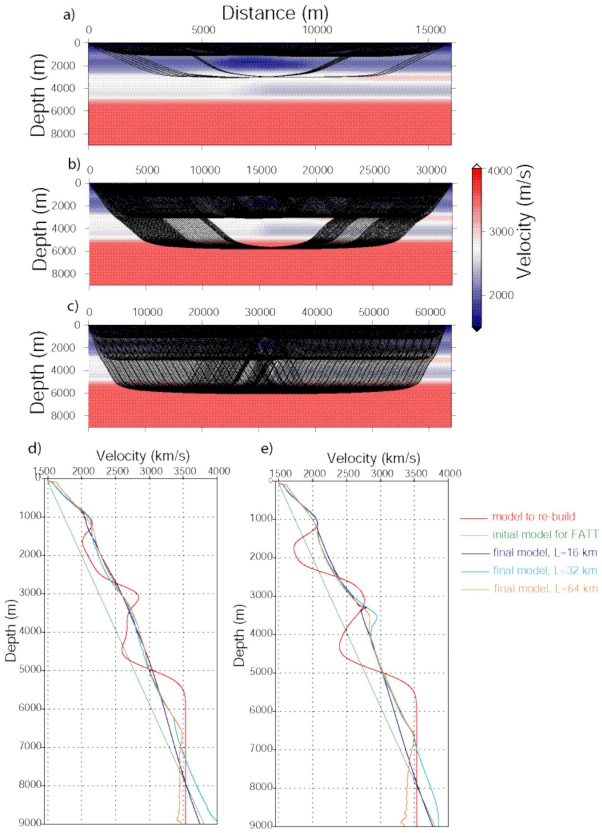

Figure 5: (a-c) First-arrival ray coverage in the smoothed Valhall velocity model for an acquisition length of 16 km (a), 32 km (b), 64 km (c). The ray coverage of the gas cloud and of the deep part of the model is improved from a) to c). (d-e) Logs extracted from the FATT models, in the middle of the model (d) and 6 km from the middle on the left (e).

Results of FWI

The final FWI velocity models inferred from the three starting models of Figures 6 are shown in Figure 8. Two FWI velocity models inferred from the same FATT starting model are shown in Figures 8(a-b). In the first test, no data damping was applied during FWI (with 40 iterations per frequency) on contrary to the second case (with 20 iterations per damping parameter). The data damping improved again the FWI model significantly. The same data damping was subsequently used when the stereotomography and the smoothed models were used as starting models (Figures 8(c-d)). Velocity logs extracted from the FWI models of Figures 8(b-d) are shown in Figure 9 at horizontal distances of 4 km and 8 km. The three starting models led to accurate FWI models down to the top of the gas cloud at 1.5 km depth. The stereotomography starting model led to the best reconstruction in the gas cloud down to 2.5-km depth in the middle of the model (Figure 9b) but the reconstruction is degraded as we move from the center of the model because of insufficient long-offset coverage used during stereotomography (Figure 9a). Within the gas cloud, the worst FWI model was inferred from the FATT starting model (Figure 9b). The comparative accuracy of the FWI reconstructions simply traduces the footprint of the three starting models in the gas cloud

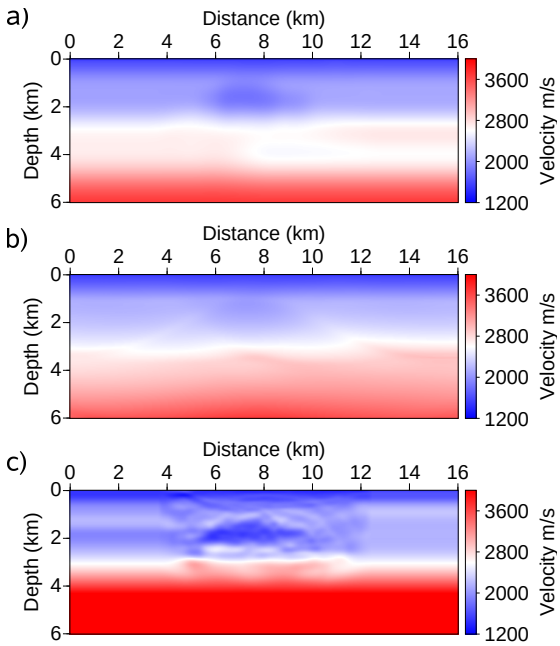

Figure 6: Initial models for FWI. a) Smoothed version of the true model, b) FATT model and c) Stereotomography model.

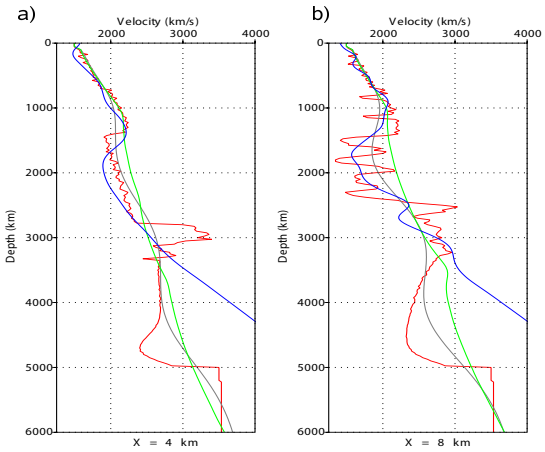

Figure 7: Logs of the FWI initial models built by smoothing of true model (gray), by FATT (green) and by stereotomography (blue). The true logs are in red. a) x=4 km. b) x=8km.

whose accuracies can be compared in Figure 7b. The fact that the most accurate velocity model was obtained from reflection traveltime tomography rather than from diving wave traveltime tomography in the LVZ associated with the gas cloud was expected. The FATT model led to reasonable FWI reconstruction below the gas cloud which illustrates the potential contribution of the long offsets to build the deep part of the model.

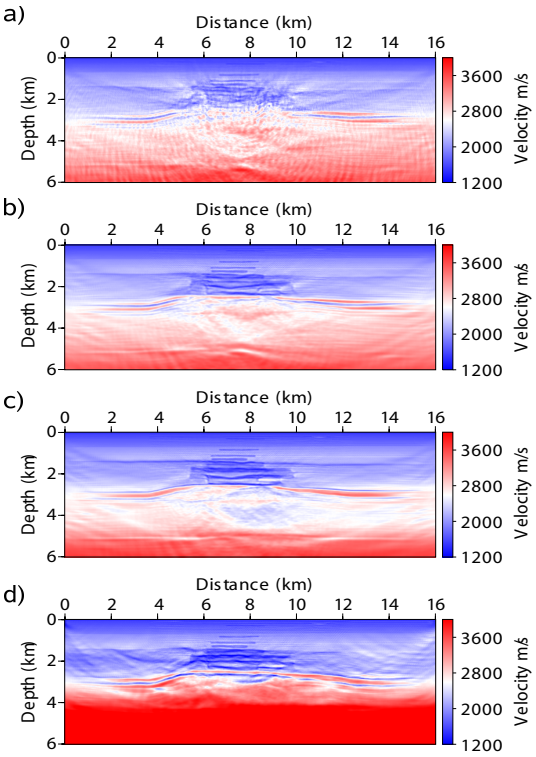

Figure 8: FWI models obtained with the initial model by FATT without data preconditioning (a), by FATT with data preconditioning (b), by Gaussian smoothing of the true model (c), and by stereotomography (d).

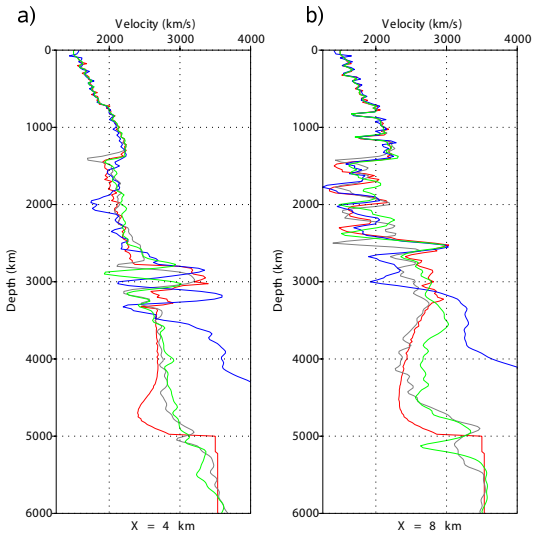

Figure 9: Logs extracted at 4 km (a) and 8 km (b) from the true model (red) and from the final FWI models using initial models built by Gaussian smoothing of the true model (gray), FATT (green) and stereotomography (blue).

CONCLUSION

We illustrate how the non linearities introduced by long-offset acquisition can be managed during frequency-domain FWI by introducing two nested hierarchical levels in the multiscale reconstruction. The first classical level consists of successive inversions of increasing frequencies. The second level proceeds from the inversion of the early arrivals to that of the later arriving phases. We apply this inversion strategy to the Valhall synthetic velocity model using three different starting models. Velocity models developed by reflection stereotomography leads to more accurate FWI models than FATT where LVZs are present in the structure. The potential benefit of long offset data in terms of aperture illumination to reconstruct the deep part of the model below the gas cloud was illustrated. Low-fold node acquisition may be the most suitable long-offset acquisition to build accurate starting model for FWI. Future works will concern assessment of refraction and reflection stereotomography and semi-global first-arrival traveltime tomography (Improta et al., 2002) as possible tools to build reliable FWI initial models from long-offset data.

ACKNOWLEDGEMENT

We thank BP for providing the Valhall velocity model. We are grateful to L. Sirgue (BP) and J. Kommedal (BP) for fruitful discussions. We thank G. Lambaré (CGG-Veritas) for providing the velocity model developed by stereotomography. This work was funded by the SEISCOPE consortium (http://seiscope.unice.fr) sponsored by BP, CGG-Veritas, Exxon-Mobil, Shell and Total. We gratefully acknowledge the access to the computer facilities provided by the SIGAMM computer center.

EDITED REFERENCES

Note: This reference list is a copy-edited version of the reference list submitted by the author. Reference lists for the 2009 SEG Technical Program Expanded Abstracts have been copy edited so that references provided with the online metadata for each paper will achieve a high degree of linking to cited sources that appear on the Web.

REFERENCES

Billette, F., and G. Lambaré, 1998, Velocity macro-model estimation from seismic reflection data by stereotomography: Geophysical Journal International, **135**, 671–680.

Brenders, A. J., and R. G. Pratt, 2007a, Efficient waveform tomography for lithospheric imaging: Implications for realistic 2D acquisition geometries and low frequency data: Geophysical Journal International, **168**, 152–170.

———, 2007b, Full waveform tomography for lithospheric imaging: Results from a blind test in a realistic crustal model: Geophysical Journal International, **168**, 133–151.

Brossier, R., S. Operto, and J. Virieux, 2008, 2D elastic frequency-domain full-waveform inversion for imaging complex onshore structures: 71st Conference and Exhibition, EAGE, Extended Abstracts.

Dessa, J. X., S. Operto, S. Kodaira, A. Nakanishi, G. Pascal, K. Uhira, and Y. Kaneda, 2004, Deep seismic imaging of the eastern Nankai Trough (Japan) from multifold ocean bottom seismometer data by combined traveltime tomography and prestack depth migration: Journal of Geophysical Research, **109**, doi:10.1029/2003JB002689.

Hustedt, B., S. Operto, and J. Virieux, 2004, Mixed-grid and staggered-grid finite difference methods for frequency domain acoustic wave modelling: Geophysical Journal International, **157**, 1269–1296.

Improta, L., A. Zollo, A. Herrero, R. Frattini, J. Virieux, and P. DellAversana, 2002, Seismic imaging of complex structures by non-linear traveltimes inversion of dense wide-angle data: application to a thrust belt: Geophysical Journal International, **151**, 264–278.

Lambaré, G., and M. Alerini, 2005, Semi-automatic pp-ps stereotomography: application to the synthetic Valhall dataset: 75th Annual International Meeting, SEG, Expanded Abstracts, **24**, 943–946.

Pratt, R. G., 1999, Seismic waveform inversion in the frequency domain, Part I: Theory and verification in a physical scale model: Geophysics, **64**, 888–901.

Pratt, R. G., C. Shin, and G. J. Hicks, 1998, Gauss-Newton and full Newton methods in frequency-space seismic waveform inversion: Geophysical Journal International, **133**, 341–362.

Sears, T. J., S. C. Singh, and P. J. Barton, 2008, Elastic full waveform inversion of multi-component OBC seismic data: Geophysical Prospecting, **56**, 843–862.

Sirgue, L., 2003, Inversion de la forme d'onde dans le domaine fréquentiel de données sismiques grand offset: PhD thesis, Université Paris and Queen's University.

Sirgue, L., 2006, The importance of low frequency and large offset in waveform inversion: 68th Conference and Exhibition, EAGE, Extended Abstracts, A037.

Sirgue, L., and R. G. Pratt, 2004, Efficient waveform inversion and imaging: a strategy for selecting temporal frequencies: Geophysics, **69**, 231–248.

Sourbier, F., S. Operto, J. Virieux, P. Amestoy, and J. Y. L'Excellent, 2009a, FWT2D: a massively parallel program for frequency-domain full-waveform tomography of wide-aperture seismic data–Part 1: Algorithm: Computer & Geosciences, **35**, 487–495.

———, 2009b, FWT2D: a massively parallel program for frequency-domain full-waveform tomography of wide-aperture seismic data–Part 2: Numerical examples and scalability analysis: Computer & Geosciences, **35**, 496--514.

Tarantola, A., 1987, Inverse problem theory: methods for data fitting and model parameter estimation: Elsevier.